J. Fluid Mech. (2010), *vol.* 645, *pp.* 279–294. © Cambridge University Press 2010
doi:10.1017/S0022112009992679

Sharp-interface limit of the Cahn–Hilliard model for moving contact lines

PENGTAO YUE[1]†, CHUNFENG ZHOU[2] AND JAMES J. FENG[2,3]

[1]Department of Mathematics, Virginia Polytechnic Institute and State University, Blacksburg, VA 24061-0123, USA

[2]Department of Chemical and Biological Engineering, University of British Columbia, Vancouver, BC V6T 1Z3, Canada

[3]Department of Mathematics, University of British Columbia, Vancouver, BC V6T 1Z2, Canada

(Received 7 October 2008; revised 9 October 2009; accepted 9 October 2009)

Diffuse-interface models may be used to compute moving contact lines because the Cahn–Hilliard diffusion regularizes the singularity at the contact line. This paper investigates the basic questions underlying this approach. Through scaling arguments and numerical computations, we demonstrate that the Cahn–Hilliard model approaches a sharp-interface limit when the interfacial thickness is reduced below a threshold while other parameters are fixed. In this limit, the contact line has a diffusion length that is related to the slip length in sharp-interface models. Based on the numerical results, we propose a criterion for attaining the sharp-interface limit in computing moving contact lines.

1. Introduction

The moving contact line is a difficult problem in interfacial fluid dynamics, since the conventional Navier–Stokes formulation runs into a non-integrable stress singularity (Dussan 1979). The crux lies in the interplay between large-scale hydrodynamics and the local molecular processes, which determines the dynamic contact angle and the velocity of the contact line. Existing theories attempt to capture one aspect of the physics and replace the others by modelling. For example, macroscopic models circumvent the stress singularity by replacing the local dynamics by the Navier slip conditions (Zhou & Sheng 1990; Haley & Miksis 1991; Spelt 2005) or a 'numerical slip' (Renardy, Renardy & Li 2001; Mazouchi, Gramlich & Homsy 2004). Microscopic models seek to compute the dynamic contact angle from the kinetics of fluid molecules jumping on the solid over an activation energy (Blake 2006). Molecular dynamics (MD) simulations probe still smaller length and time scales at the contact line (Koplik, Banavar & Willemsen 1988; Thompson & Robbins 1989; Qian, Wang & Sheng 2003). However, none of these encompasses the widely disparate length scales. More in-depth discussion of the outstanding issues can be found in recent reviews (Pismen 2002; Blake 2006; Qian, Wang & Sheng 2006*b*).

This paper concerns a 'mesoscopic' approach to the moving-contact-line problem using the so-called diffuse-interface or phase-field theory, originally proposed by van der Waals (1892). The interface is treated as a diffuse layer through which the

† Email address for correspondence: ptyue@math.vt.edu

fluid properties vary steeply but continuously. By expanding the density distribution function in space and then truncating and integrating the intermolecular forces, one coarse-grains the microscopic physics at the contact line into fluid–fluid and fluid–substrate interaction energies. These are then incorporated into the hydrodynamics via a variational procedure (Pismen 2002). On this mesoscopic scale, the motion of the contact line occurs naturally as diffusion across the interface driven by gradients of the chemical potential or concentration. There is no longer a singularity. Meanwhile, being a continuum theory, the diffuse-interface model is capable of computing macroscopic flows in complex geometry. Because of these attractive features, several groups have applied the Cahn–Hilliard version of the model, called the CH model hereafter, to contact-line problems, e.g. Seppecher (1996), Jacqmin (2000), Villanueva & Amberg (2006), Khatavkar, Anderson & Meijer (2007), Ding & Spelt (2007) and Huang, Shu & Chew (2009).

But there are difficulties, both conceptual and technical, facing this approach. When the CH model is used to compute interfacial flows without contact lines, the underlying assumption is to approach the so-called sharp-interface limit (Caginalp & Chen 1998; Lowengrub & Truskinovsky 1998). Mathematically, this relates the diffuse-interface picture to the classical Navier–Stokes description of internal boundaries of zero thickness. Computationally, this provides a sort of 'convergence criterion' for diffuse-interface computations, which typically use interfaces much thicker than the real ones (Khatavkar, Anderson & Meijer 2006). The hydrodynamic results become definite and meaningful only if they no longer depend on the interfacial thickness, that is to say when the sharp-interface limit is reached (Yue *et al.* 2006).

For the moving-contact-line problem, however, the sharp-interface limit has not yet been firmly established (Wang & Wang 2007). This is a severer deficiency than would be for non-contact-line problems. For the latter, the diffuse interface is chiefly a numerical device for capturing moving interfaces (Yue *et al.* 2004); the Cahn–Hilliard diffusion within the interfacial region is of little interest and indeed dies out as the interface gets thinner. For a moving contact line, however, the Cahn–Hilliard diffusion embodies key molecular processes that determine the contact-line speed and the dynamic contact angle. Does this picture have a well-defined sharp-interface limit? If yes, is this limit physically meaningful?

A survey of the literature shows that these questions have never been seriously studied before. Prior computational work is concerned primarily with implementing the Cahn–Hilliard formalism in algorithm and reproducing 'qualitative' features of the process. The objectives of the present study are to (*a*) establish the sharp-interface limit for the moving-contact-line problem, (*b*) demonstrate a connection between this limit and the conventional idea of slip and (*c*) provide practical guidelines for attaining that limit computationally.

2. Theoretical model

Consider a system of two nominally immiscible Newtonian fluids in contact with each other and with a solid surface (figure 1). We introduce a scaled 'concentration' ϕ such that in the two-fluid bulks $\phi = \pm 1$ and the fluid–fluid interface is given by $\phi = 0$. Denoting the fluid domain by Ω and the solid surface by $\partial\Omega$, we write the free energy of the system as

$$\mathscr{F} = \int_{\Omega} f_m(\phi, \nabla\phi)\,\mathrm{d}\Omega + \int_{\partial\Omega} f_w(\phi)\,\mathrm{d}A, \tag{2.1}$$

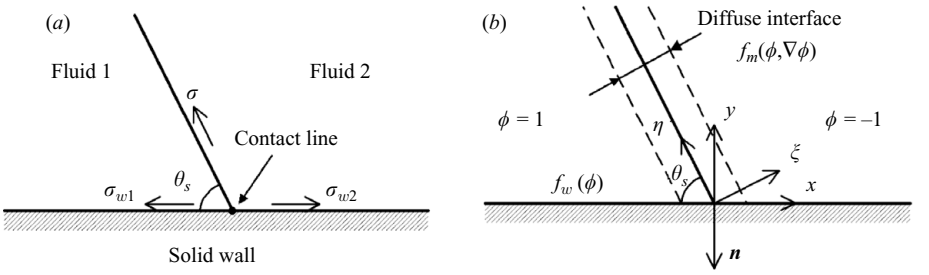

FIGURE 1. A static contact line viewed in (*a*) the sharp-interface model and (*b*) the diffuse-interface model: $\boldsymbol{n}$ is the outward normal to the wall and ξ is the normal to the interface; other symbols are defined in the text.

where the fluid–fluid mixing energy (Cahn & Hilliard 1958)

$$f_m(\phi, \nabla\phi) = \frac{\lambda}{2}|\nabla\phi|^2 + \frac{\lambda}{4\epsilon^2}(\phi^2 - 1)^2 \tag{2.2}$$

and the wall energy (Cahn 1977; Jacqmin 2000)

$$f_w(\phi) = -\sigma\cos\theta_S\frac{\phi(3-\phi^2)}{4} + \frac{\sigma_{w1}+\sigma_{w2}}{2}. \tag{2.3}$$

In f_m, λ is the mixing energy density and ϵ is the capillary width, and in equilibrium the fluid–fluid interfacial tension is given by

$$\sigma = \frac{2\sqrt{2}}{3}\frac{\lambda}{\epsilon}. \tag{2.4}$$

The wall energy is designed so that away from the contact line, $f_w(\pm 1)$ gives the fluid–solid interfacial tensions σ_{w1} and σ_{w2} for the two fluids, which determine the static contact angle θ_S through Young's equation $\sigma_{w2} - \sigma_{w1} = \sigma\cos\theta_S$. In equilibrium, minimizing $\mathscr{F}$ shows that ϕ contours are parallel lines intersecting the wall at the angle θ_S. Along the normal to the interface ξ, ϕ retains its characteristic hyperbolic-tangent profile, undisturbed by f_w. Note that with this energy formulation, it is numerically difficult to accurately reproduce a θ_S close to 0° or 180°, and the model cannot handle precursor films.

A variational procedure (Jacqmin 2000; Qian, Wang & Sheng 2006*a*) leads to the bulk chemical potential $G = \lambda\left[-\nabla^2\phi + (\phi^2-1)\phi/\epsilon^2\right]$ and a 'body force' $\boldsymbol{B} = G\nabla\phi$ that is the diffuse-interface equivalent of the interfacial tension (Yue *et al.* 2006). Now we can write out the Navier–Stokes and Cahn–Hilliard equations for the CH model:

$$\nabla\cdot\boldsymbol{v} = 0, \tag{2.5}$$

$$\rho\left(\frac{\partial\boldsymbol{v}}{\partial t} + \boldsymbol{v}\cdot\nabla\boldsymbol{v}\right) = -\nabla p + \nabla\cdot\left[\mu\left(\nabla\boldsymbol{v} + (\nabla\boldsymbol{v})^T\right)\right] + G\nabla\phi, \tag{2.6}$$

$$\frac{\partial\phi}{\partial t} + \boldsymbol{v}\cdot\nabla\phi = \nabla\cdot(\gamma\nabla G). \tag{2.7}$$

In the momentum equation, the density ρ and viscosity μ are algebraic averages of the fluid components. The Cahn–Hilliard equation describes the convection-diffusion of the species, with a diffusive flux proportional to the gradient of G, the coefficient γ being the mobility parameter. These are supplemented by the following boundary

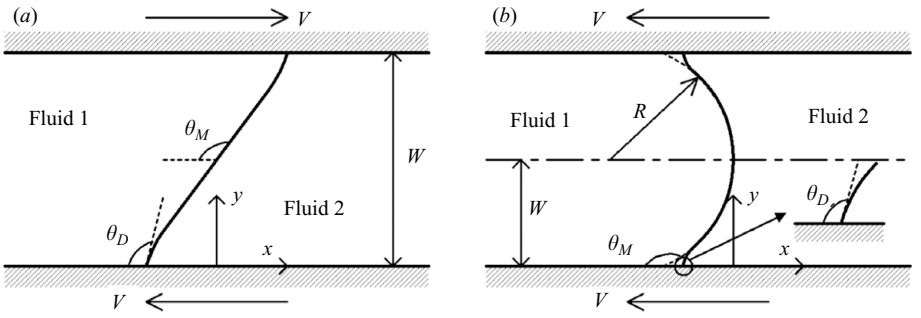

FIGURE 2. Steady (*a*) Couette and (*b*) Poiseuille flows of two immiscible fluids, viewed in a reference frame attached to the steadily moving contact line: θ_D is the microscopic dynamic contact angle and θ_M is a suitably defined apparent contact angle. Through (2.10), we assume fluid–solid equilibrium on the substrate and $\theta_D = \theta_S$.

conditions on the solid substrate $\partial\Omega$:

$$\boldsymbol{v} = \boldsymbol{v}_w, \tag{2.8}$$

$$\boldsymbol{n}\cdot\nabla G = 0, \tag{2.9}$$

$$\lambda\boldsymbol{n}\cdot\nabla\phi + f_w'(\phi) = 0, \tag{2.10}$$

where $\boldsymbol{v}_w$ is the wall velocity. The second condition, zero flux through the solid wall, is self-evident. The no-slip condition implies that the motion of the contact line is entirely due to the Cahn–Hilliard diffusion. It is possible to introduce a slip velocity here (Qian *et al.* 2006*b*), which would allow more freedom in fitting the data and perhaps also a better representation of the true physics. Given the objectives of the present work, however, it seems reasonable to restrict the number of parameters to a minimum. Equation (2.10) is the natural boundary condition arising from the variation of the wall energy f_w. It represents a local equilibrium at the wall and constrains the dynamic contact angle θ_D to the static value θ_S to the leading order (Jacqmin 2000). This condition may be generalized to include wall relaxation and to allow θ_D to deviate from θ_S. Though a key idea to molecular-kinetic modelling and MD simulations (Qian *et al.* 2003, 2006*b*; Blake 2006), we will not consider wall relaxation in this work.

3. Dimensionless groups

We consider steady Couette and Poiseuille flows in a reference frame in which the walls are in motion but the interface is stationary (figure 2). The former corresponds to shearing between two parallel planes, while the latter corresponds to the displacement of one fluid by another in a capillary tube. The length of the computational domain is $4W$ for Couette flow and $6W$ for Poiseuille flow; these are sufficiently long such that the interface does not affect the inflow and outflow conditions. As contact-line dynamics is most significant for slow flows, we neglect inertia. Then the independent parameters of the problem are channel width or tube radius W, velocity V, component viscosities μ_1 and μ_2, static contact angle θ_S, mixing energy density λ, capillary width ϵ and interfacial mobility parameter γ. Note that σ is given by (2.4). Out of these,

five dimensionless groups can be constructed:

$$Ca = \frac{\mu_1 V}{\sigma} \quad \text{(capillary number)}, \tag{3.1}$$

$$\mu^* = \frac{\mu_2}{\mu_1} \quad \text{(viscosity ratio)}, \tag{3.2}$$

$$Cn = \frac{\epsilon}{W} \quad \text{(Cahn number)}, \tag{3.3}$$

$$S = \frac{\sqrt{\gamma \mu_1}}{W}, \tag{3.4}$$

$$\theta_S \qquad \text{(static contact angle)}. \tag{3.5}$$

In the literature, a Péclet number $Pe = VW\epsilon/(\gamma\sigma)$ is sometimes used instead of S (e.g. Villanueva & Amberg 2006; Khatavkar *et al.* 2007). It will soon become clear that S reflects the diffusion length scale at the contact line and is therefore more appropriate for our purpose.

The key observable of the problem is the interfacial shape and in particular the apparent contact angle θ_M. For Couette flow (figure 2*a*), θ_M is defined as the angle of interfacial inclination at the centre of the channel (Thompson & Robbins 1989). For Poiseuille flow (figure 2*b*), the interface assumes a spherical shape at the centre, and we define θ_M by extrapolating the spherical cap to the walls (Hoffman 1975; Fermigier & Jenffer 1991): $\theta_M = \cos^{-1}(W/R)$, R being the radius of the spherical cap. Now θ_M can be expressed as a function of the dimensionless groups:

$$\theta_M = f(Ca, \mu^*, \theta_S, Cn, S). \tag{3.6}$$

Among these, Ca, μ^* and θ_S are the same as in sharp-interface models, while Cn and S, which represent interfacial thickness and the Cahn–Hilliard diffusion respectively, are specific to the CH model. Their values are not easily assessed for real materials and hence are somewhat uncertain, and their roles in the moving contact line will be the focus of the rest of the paper. First, we examine the relationship between S and Cn in order to achieve the sharp-interface limit. This establishes a protocol that ensures convergence of the numerical result towards a definite solution. Second, we compare the sharp-interface limit with the theory of Cox (1986) to show that this limit is physically meaningful.

These are accomplished by numerical computation and scaling arguments. The computation uses Galerkin finite elements on an adaptive triangular grid that adequately resolves the interfacial region. The Navier–Stokes and Cahn–Hilliard equations are integrated using a second-order accurate, fully implicit time-marching scheme. Details of the numerical algorithm and validation can be found in Yue *et al.* (2006).

4. The sharp-interface limit

Real interfaces have a thickness of the order of nanometres. Thus, to simulate the dynamics of a 1 mm drop while resolving the Cahn–Hilliard diffusion within a 1 nm interface, the diffuse-interface method would have to bridge six decades of length scales. This is much beyond the capability of current computers and algorithms. Fortunately, the diffuse interface between two 'bulk fluids' mathematically converges to a unique sharp-interface limit when $Cn \to 0$, and this limit can be attained for $Cn = O(10^{-2})$ in practice. This is amply computable, especially with the help of adaptive meshing (Yue *et al.* 2006). Such an upper bound on Cn restricts the physical size of the problems that can be simulated. Nevertheless, the existence of the

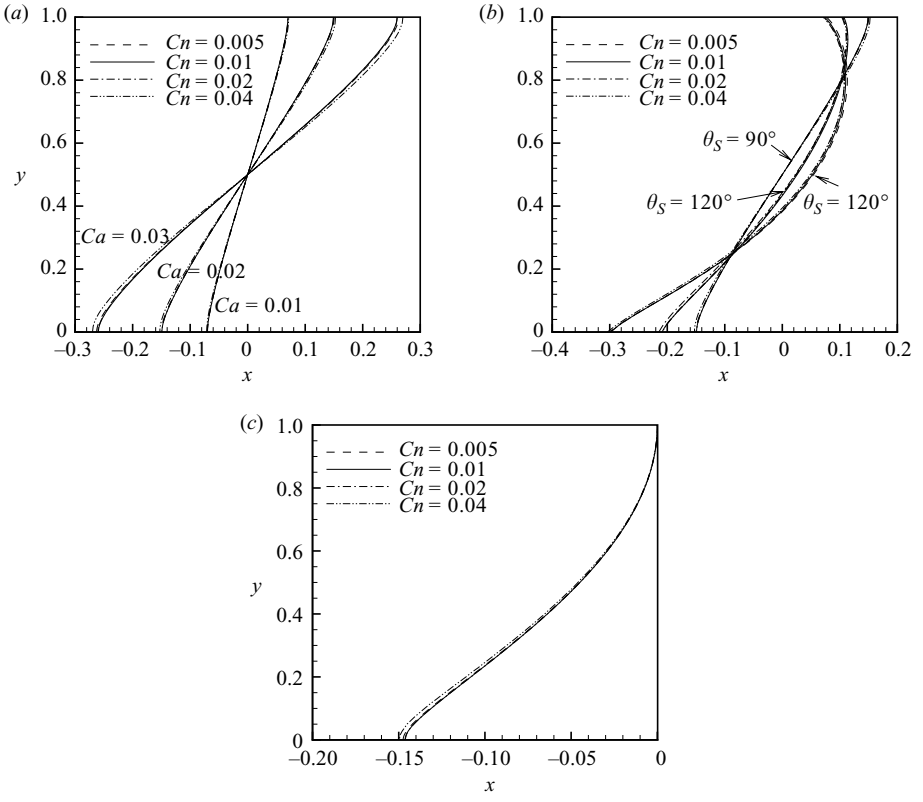

FIGURE 3. Convergence of the moving contact line to the sharp-interface limit with decreasing Cn. (a) Steady interfacial shapes in Couette flow for three Ca values with $S = 0.01$ and $\theta_s = 90°$ fixed. (b) Couette flow for three θ_S values with $S = 0.01$ and $Ca = 0.02$ fixed. (c) Poiseuille flow with $Ca = 0.02$, $S = 0.01$ and $\theta_s = 90°$ fixed. In all plots, x is the flow direction. For Couette flows, the walls are at $y = 0$ and 1. For Poiseuille flows, the tube wall is at $y = 0$ and the centre at $y = 1$. In all cases, viscosity ratio $\mu^* = 1$.

sharp-interface limit ensures that computations using sufficiently small Cn produce physically meaningful, converged solutions that can be compared with experiments and sharp-interface calculations.

If the fluid–fluid interface intersects a solid wall and forms a contact line, the situation becomes much murkier. Previous computations used Cn ranging from 5×10^{-3} to 0.3 (e.g. Jacqmin 2000, 2004; Ding & Spelt 2007), but the question of convergence to a sharp-interface limit was never raised. Using matched asymptotic expansions in Cn, Wang & Wang (2007) probed the limiting behaviour near the contact line. To the leading order, the outer solution prevailing outside the interface is shown to behave regularly, with no diffusion-induced slip on the wall. The inner solution, which would have given the diffusive flux at the contact line and hence the contact-line speed, was not given. Thus, it remains unclear whether a unique sharp-interface limit exists for the CH model for the moving contact line.

4.1. *Numerical results*

Through numerical experiments, we have gathered empirical evidence for the existence of the sharp-interface limit and have developed a practical guideline about achieving it using finite Cn. Figure 3 demonstrates that when Cn is reduced while all other

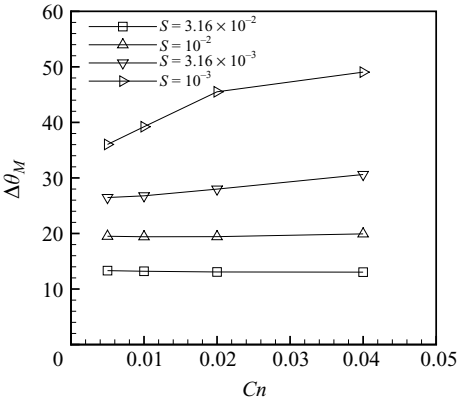

FIGURE 4. Variation of the apparent contact angle in Couette flow with Cn (representing the interfacial thickness) and S (representing the mobility parameter): $\theta_S = 90°$, $Ca = 0.02$, $\mu^* = 1$ and $\Delta\theta_M$ is defined as $\theta_M - \theta_S$.

parameters, including S, are kept constant, the interface converges to a unique shape. This has been verified for Couette and Poiseuille flows at several Ca, θ_S and μ^* values.

From figure 3, it seems reasonable to take $Cn^c = 0.01$ or 0.02 to be the threshold for convergence to the sharp-interface limit; these values are consistent with those for flows without contact lines (Yue *et al.* 2006). However, a more careful examination shows that Cn^c varies with S. In figure 4, we plot the apparent contact angle θ_M with decreasing Cn for four different S values. For the largest $S = 3.16 \times 10^{-2}$, θ_M is constant for all Cn values tested, and so $Cn^c > 0.04$. For the smallest $S = 10^{-3}$, on the other hand, even the smallest $Cn = 5 \times 10^{-3}$ is too large for convergence. Based on convergence for the two intermediate S values, we propose

$$Cn^c = 4S \tag{4.1}$$

as a guideline for approaching the sharp-interface limit. With μ^* around 1, we have tested other values of Ca and θ_S, also in Poiseuille flows. This threshold applies in all these cases. For μ^* values far from unity, the factor 4 must be modified to include μ^* because S is defined using μ_1, but μ_2 contributes to the dynamics as well. We will return to this point at the end of § 4 and suggest an 'effective viscosity' for formulating the threshold Cn^c.

It may seem natural that the sharp-interface limit should be approached by reducing Cn while keeping S constant. But this contrasts with a scaling idea in the literature. In simulating interfacial flows without contact lines, many reasoned that since the diffuse-interface model uses an artificially thick ϵ, the Cahn–Hilliard mobility parameter γ should be adjusted somehow to compensate for it (Jacqmin 1999). Therefore, γ should obey a scaling law with respect to ϵ for the model to yield consistent results at different ϵ values and to attain the sharp-interface limit. A power-law scaling $\gamma \sim \epsilon^n$ has been proposed, with the index ranging from $n = -1$ to $n = 2$ for different flow situations (Khatavkar *et al.* 2006; Yue, Zhou & Feng 2007). For the moving-contact-line problem, Jacqmin (2000) used $\gamma \sim \epsilon$ but did not offer a justification or verification. In fact, figure 3 of his work indicates a lack of convergence towards a steady-state interface when γ and ϵ approach zero at the same rate. We have tested the different power laws for the Couette flow geometry, and figure 5 shows unequivocally that only $\gamma \sim \epsilon^0$ or $S \sim Cn^0$ leads to convergence

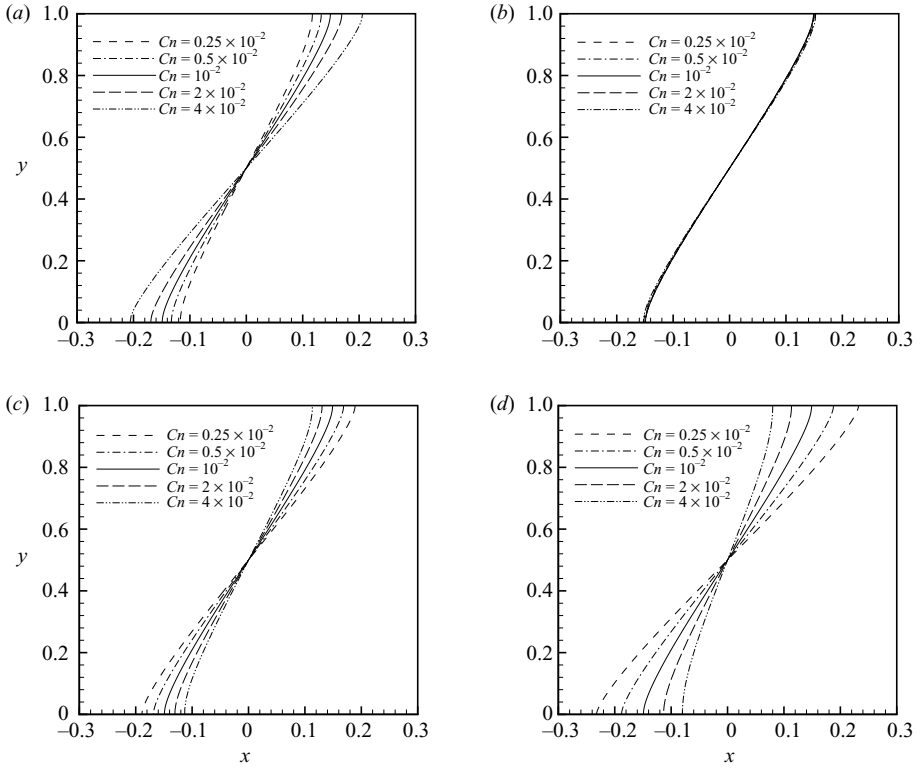

FIGURE 5. Testing the scaling laws $\gamma \sim \epsilon^n$ (i.e. $S \sim Cn^{n/2}$) for steady interface shapes in Couette flow: $Ca = 0.02$, $\theta_s = 90^\circ$ and $\mu^* = 1$ are fixed, while Cn and S are varied with respect to the baseline $Cn = 0.01$ and $S = 0.01$. (*a*) $n = -1$; (*b*) $n = 0$; (*c*) $n = 1$; (*d*) $n = 2$.

to the sharp-interface limit. With $Cn \to 0$, $n = -1$ tends to produce a limiting behaviour of a vertical interface (figure 5*a*), with perfect slip at the contact line as the Cahn–Hilliard mobility tends to infinity. Conversely, the interface for $n = 1$ or 2 tends to a 'immobilized contact line' with zero slip (figure 5*c*, *d*), as Cahn–Hilliard diffusion vanishes. The latter corresponds to the asymptotic analysis of Jacqmin (2000), where the inner solution collapses as $\epsilon \to 0$ and $\gamma \to 0$. As explained later, the curves in figure 5(*a*, *c*, *d*) may be seen as corresponding to different 'effective slip lengths'.

4.2. *Scaling arguments*

We now offer scaling arguments that explain why the sharp-interface limit is approached by $S \sim Cn^0$ but not the other power laws. It is well recognized that the diffuse interface has two inherent length scales: ϵ representing the interfacial thickness and a much larger length scale over which the Cahn–Hilliard diffusion takes place (Chen, Jasnow & Viñals 2000; Jacqmin 2000; Briant & Yeomans 2004). We will call the latter the diffusion length l_D. Thus, ϕ varies over ϵ, while the chemical potential G and flow velocity u vary over l_D (see the Appendix for a detailed explanation). One can derive scaling relationships for G and l_D at the contact line from force and mass balances ((2.6) and (2.7)). Note that p varies sharply across the interface, but outside l_D it is essentially a constant. Thus, ∇p drops out if we integrate

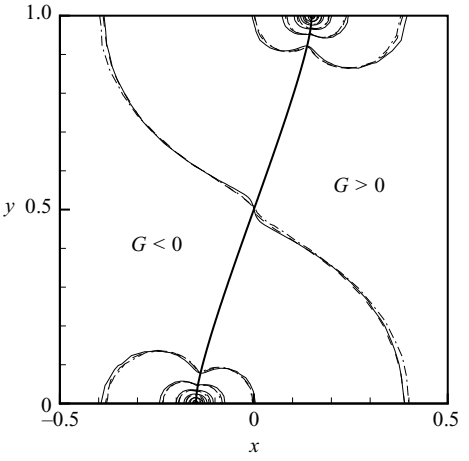

FIGURE 6. Contours of the chemical potential G in Couette flow: $Ca = 0.02$, $S = 0.01$, $\theta_S = 90°$, $\mu^* = 1$. The solid, dashed and dash-dotted lines are the contours for $Cn = 0.01$, 0.005 and 0.025, respectively. The thick line describes the location of interface.

(2.6) along the wall from $x = -l_D$ to l_D (cf. figure 2):

$$\int_{-l_D}^{l_D} \left(G\frac{\partial \phi}{\partial x} + \mu \frac{\partial^2 u}{\partial x^2} \right) \mathrm{d}x = 0, \tag{4.2}$$

where we have omitted inertia. Using the maximum G_{max} to represent the magnitude of G and noting that ϕ varies over order one, we obtain

$$G_{max} \sim \frac{\mu V}{l_D}. \tag{4.3}$$

For brevity, we have used the same μ to denote the characteristic viscosity near the interface; it may be one of the component viscosities or their average. Similarly, integrating the Cahn–Hilliard equation (2.7) along the wall from $x = -l_D$ to $x = l_D$ produces a balance between the convective flux across the interface $\boldsymbol{v}\phi \sim V$ and the diffusive flux $\gamma \nabla G \sim \gamma G_{max}/l_D$:

$$V \sim \frac{\gamma G_{max}}{l_D}. \tag{4.4}$$

Combining the above scalings, we get

$$l_D \sim \sqrt{\gamma \mu} \tag{4.5}$$

and

$$G_{max} \sim \frac{\mu V}{\sqrt{\gamma \mu}}. \tag{4.6}$$

Note that in our nomenclature, we have assigned the bulk values of ϕ to ± 1. Other authors have adopted different conventions, say with $\phi = \pm\alpha$ in the bulk phases (Jacqmin 2000). Then the diffusion length should be written as $\sqrt{\gamma\mu}/\alpha$.

These scalings support the observations that the sharp-interface limit is approached by keeping S (or γ) constant while reducing Cn (or ϵ). Neither G_{max} nor l_D depends on ϵ. Therefore, there is no need to compensate for a thicker ϵ by adjusting the Cahn–Hilliard diffusion. The scaling has been verified by our numerical simulations. With Cn decreasing from 0.01 to 0.0025 and $S = 0.01$ and $Ca = 0.02$ fixed, G contours around the contact line stay essentially unchanged (figure 6), as does the

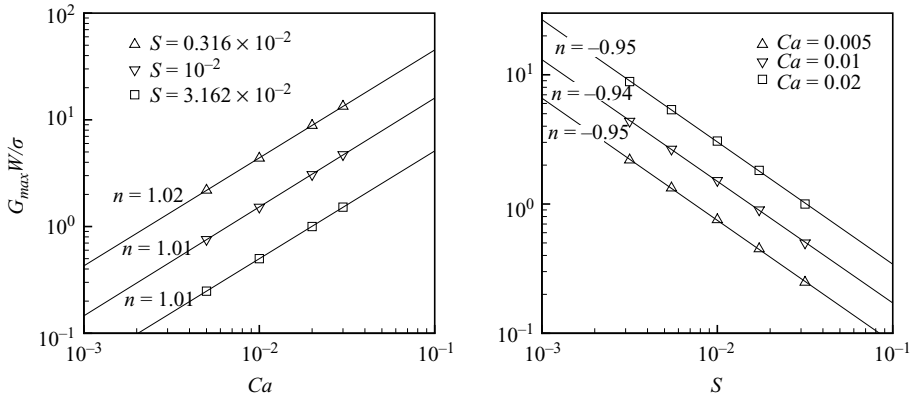

FIGURE 7. Numerical verification of the scaling relationship of (4.7) in the Couette flow. (*a*) Variation of G_{max} with Ca for several S values. (*b*) Variation of G_{max} with S for several Ca values. In both plots, $Cn = 0.01$, $\theta_S = 90^\circ$, $\mu^* = 1$. The straight lines are power-law fittings with the index n labelled in the plots.

velocity field. This unique converged solution is the sharp-interface limit. Besides, we have varied V and γ systematically to confirm (4.6), which in dimensionless form may be written as

$$\frac{G_{max}}{\sigma/W} \sim \frac{Ca}{S}. \tag{4.7}$$

Figure 7 clearly demonstrates the proportionality of G_{max} with Ca/S.

4.3. *Diffusion length*

The significance of the diffusion length l_D warrants further discussion. First, (4.5) is the same as suggested by Jacqmin (2000) based on dimensions. But it differs from the scaling derived by Briant & Yeomans (2004),

$$l_D \sim (\gamma \mu \epsilon^2)^{1/4}, \tag{4.8}$$

which is based on balancing the viscous and interfacial forces 'locally' at a spatial point. This ignores the order-one effect of ∇p, which we have handled by integrating in (4.2).

Second, Jacqmin (2000) showed that in the asymptotic limit of $Ca \to 0$, $l_D \to 0$ and $\epsilon/l_D \to 0$, l_D can be related to the 'slip length' l_s in the sharp-interface analysis of Cox (1986). Note that Jacqmin's limit is an immobile contact line, as he required both γ and ϵ approaching zero; it is not the sharp-interface limit as defined here. Nevertheless, our computations show that this connection between l_D and l_s holds in our case as well. In fact, it extends to the entire range of Ca, up to the critical value for wetting failure. This is illustrated in figure 8 in terms of the apparent contact angle θ_M. Cox (1986) expressed θ_M in a celebrated formula:

$$g(\theta_M, \mu^*) = g(\theta_S, \mu^*) + Ca \ln(\delta^{-1}), \tag{4.9}$$

where g is a complex but known function given in the original paper and $\delta = l_s/W$ is the ratio between the slip length and the macroscopic length. If we equate our $S = l_D/W$ to Cox's δ, then the CH model predicts $\theta_M(Ca)$ curves in close agreement with Cox's formula. The physical meaning of this correspondence can be made more precise by studying the local flow field surrounding the contact line (figure 9). For all Ca, S and θ_S values tested in Couette and Poiseuille flows, the stagnation point always

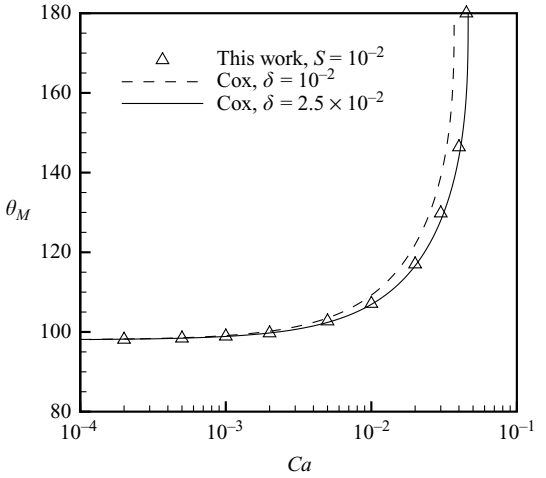

FIGURE 8. Close agreement between $\theta_M(Ca)$ predicted by the CH model and the theory of Cox (1986) in Poiseuille flow, with Cox's slip length l_s equated to the Cahn–Hilliard diffusion length l_D (dashed curve) or $2.5l_D$ (solid curve): $\theta_S = 98^\circ$, $\mu^* = 0.9$ and $Cn = 0.01$. Around $Ca = 0.05$, $\theta_M \to 180^\circ$ indicates the onset of wetting failure.

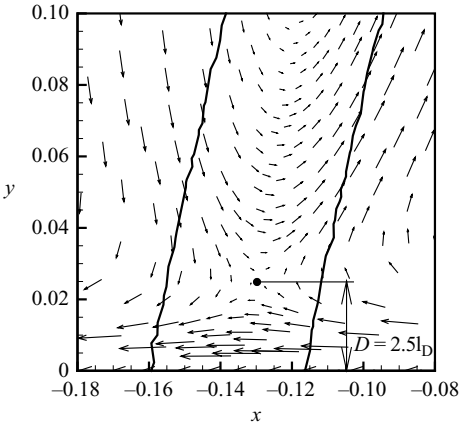

FIGURE 9. Steady-state velocity field near the contact line in Poiseuille flow: $\theta_S = 98^\circ$, $\mu^* = 0.9$, $Ca = 0.02$, $Cn = 0.01$ and $S = 0.01$. The solid lines are the level sets of $\phi = \pm 0.9$, and the black dot indicates the stagnation point. Note that the level sets of ϕ are essentially parallel curves once the sharp-interface limit is attained. Over a larger length scale, the flow field manifests the characteristic wedge-flow pattern of Huh & Scriven (1971).

sits at approximately the same distance ($D \approx 2.5l_D$) from the wall provided that Cn is small enough to attain the sharp-interface limit. This distance is consistent with the calculations of Jacqmin (2000). If one views the flow between the wall and the stagnation point as 'slip' of the contact line, then $D \approx 2.5l_D$ bears the concrete meaning of the slip length. Furthermore, if we equate $2.5l_D$ with Cox's slip length l_s (or in dimensionless form $\delta = 2.5S$), then Cox's formula falls almost precisely on the Cahn–Hilliard prediction (figure 8). This confirms more quantitatively the correspondence between $D = 2.5l_D$ and the slip length l_s in the sharp-interface context.

To further elucidate the connection between l_D and l_s, we explore the asymptotic behaviour of the apparent contact angle in the CH model as l_D decreases towards

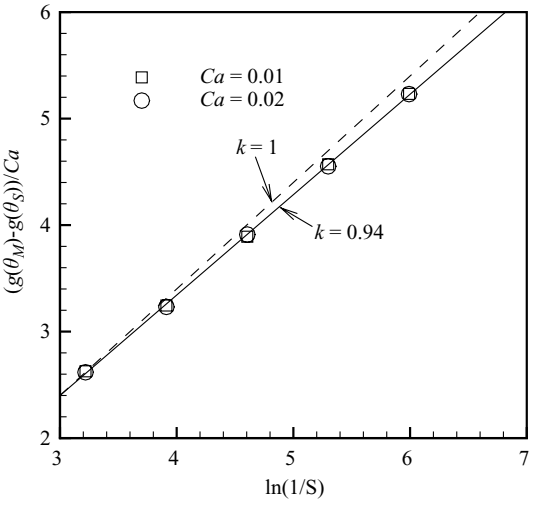

FIGURE 10. Verification of the logarithmic behaviour of θ_M in the CH model. The computation is for a Poiseuille flow with $Cn = 0.005$, $\mu^* = 0.9$ and $\theta_S = 98°$. The best linear fitting has a slope of $k = 0.94$.

zero. To guarantee that the interfacial thickness falls in the sharp-interface limit for the smallest l_D tested, we choose $Cn = 0.005$ instead of $Cn = 0.01$. Figure 10 clearly shows the logarithmic divergence of Cox's formula, and both numerical data sets fall on the same straight line. Note that the slope $k = 0.94$ is slightly below Cox's formula ($k = 1$), and the intercept corresponds to $-\ln(1.5S)$ rather than $-\ln(2.5S)$. Nevertheless, the CH model manifests an asymptotic behaviour that largely agrees with Cox's formula.

Finally, the physical picture for l_D – as the Cahn–Hilliard diffusion length as well as the effective slip length – gives additional meaning to the threshold Cn^c (4.1) for attaining the sharp-interface limit. Since $Cn/S = \epsilon/l_D$, requiring this ratio to be below an upper bound amounts to requiring the diffusion length to be 'resolved' by an adequate number of the capillary width ϵ. This is reminiscent of the finding of Zhou & Sheng (1990) in their sharp-interface calculations with slip models that one needs a sufficient number of grid points inside the slip region to ensure accuracy of the solution. What is surprising is the numerical factor $Cn^c/S = 4$. In the physical picture of the diffuse interface, one expects l_D to be much larger than ϵ. Thus, $Cn^c = 4S$ is a remarkably forgiving criterion. It implies that the Cahn–Hilliard result converges to the sharp-interface limit for interfaces as thick as many times of l_D.

So far, we have presented results for viscosity ratio μ^* equal or close to one. For highly dissimilar viscosities, the diffusion length l_D has to be modified to include μ^*. Calculations show that the stagnation point in figure 9 migrates towards the less viscous component and the solid wall, with a recirculating eddy on the less viscous side, similar to the findings of Sheng & Zhou (1992). Thus, stronger shear takes place in the less viscous region, and the result is more sensitive to the lower viscosity. Figure 11 shows that the observation $D \approx 2.5l_D$ still holds if we use an 'effective viscosity' $\mu_e = \sqrt{\mu_1\mu_2}$ to define $l_D = \sqrt{\mu_e\gamma}$. The redefined l_D retains its connection to the stagnation point and hence to the slip length l_s for all values of μ^* tested. Furthermore, numerical tests confirm that the criterion for convergence to the sharp-interface limit, $\epsilon = 4l_D$ or $Cn^c = 4S$ (4.1), remains valid if l_D and S are redefined using

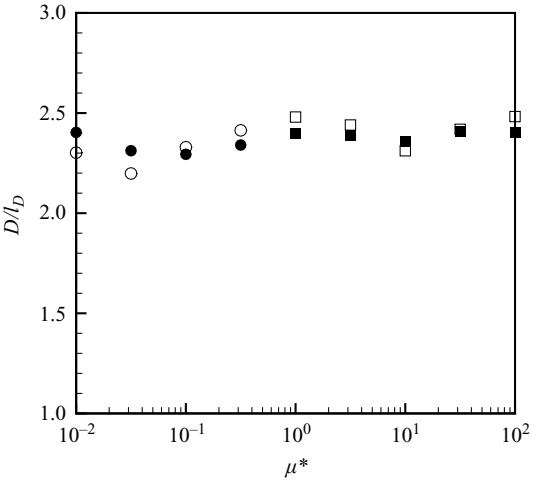

FIGURE 11. Position of the stagnation point as a function of viscosity ratio in Poiseuille flow: D is the distance between the stagnation point and the wall; l_D is redefined as $l_D = \sqrt{\mu_e \gamma}$, where $\mu_e = \sqrt{\mu_1 \mu_2}$ is the effective viscosity; $\theta_S = 90°$; $Cn = 5 \times 10^{-3}$. The symbols represent different schemes in varying the viscosities and S. The circles are for a fixed $Ca = 0.01$, with the open and closed circles at $S = 0.01$ and 0.02, respectively. The squares correspond to $Ca/\mu^* = 0.01$ being fixed, with the open and closed squares at $S/\sqrt{\mu^*} = 0.01$ and 0.02, respectively.

μ_e. Therefore, all conclusions drawn from equal-viscosity systems can be extended to unequal-viscosity systems by replacing μ with μ_e.

5. Conclusions

Diffuse-interface models regularize the stress singularity at the moving contact line and offer a straightforward route for conducting flow simulations. For the results to be meaningful and useful, however, such simulations must produce definite and converged results in a self-consistent way. Through theoretical analysis and numerical simulations of the CH model, we have clarified and explained the behaviour of the model and have produced practical guidelines for numerical simulations. The main results can be summarized as follows.

(*a*) The CH model has a sharp-interface limit that is approached by reducing the interfacial thickness while keeping all other parameters fixed.

(*b*) There is a deep connection between the CH model and the theory of Cox (1986). The CH model predicts a diffusion length scale for the contact line $l_D = \sqrt{\gamma \mu}$, which corresponds to the slip length l_s in the Cox theory. It is this l_D, rather than the interfacial thickness, that controls the contact-line dynamics.

(*c*) To attain the sharp-interface limit, the capillary width of the interface should satisfy $\epsilon < 4l_D$. This is recommended as a guideline for producing convergent results for the moving contact line.

As a local model for the contact line, the CH model enjoys two advantages over the Cox model. First, it replaces the *ad hoc* slip condition with Cahn–Hilliard diffusion that can, to a good degree, be interrogated for physical insights. Thus, the CH model employs a deeper phenomenology, which, through the notions of viscous bending and wall relaxation, integrates hydrodynamic and molecular-kinetic ideas and is therefore more comprehensive than the Cox model. Second, the diffuse interface is

also a computational tool for interfacial flows. Unlike the asymptotic Cox theory, for example, the CH model applies to large-scale flows at finite Ca in complex geometries.

As compared with slip-based computations using other interface-capturing schemes, a unique advantage of the CH model is that it captures the interface and regularizes the moving contact line by using a single scalar ϕ field.

A potential limitation of the CH model for computing moving contact lines, and to a lesser degree for computing other interfacial flows, is the need to use artificially large ϵ and l_D values. Real interfaces have a thickness of the nanometre scale. Typical slip and diffusion lengths at the contact line are roughly in the same range. Thus, if the macroscopic scale of the problem exceeds say hundreds of microns, the span of length scales becomes too wide for today's computing capability. This raises new questions. Is it possible for the CH model to quantitatively predict macroscopic behaviour of moving contact lines by using numerically manageable ϵ and l_D? If so, what are the upper bounds for these parameters? These questions should be investigated in future work.

We acknowledge support by the Petroleum Research Fund, the Canada Research Chair program, NSERC, CFI and NSFC (Grant Nos. 50390095, 20674051). Part of this work was done during JJF's visit at the Kavli Institute for Theoretical Physics in Beijing. We thank T. Qian, X.-P. Wang and Y.-G. Wang for stimulating discussions.

Appendix. Length scale of chemical potential G

Although often assumed in the literature, the fact that G varies over a length scale different from ϕ has apparently never been justified explicitly. Here we provide a simple explanation.

Across a planar interface at equilibrium, $G=0$ everywhere and ϕ assumes a hyperbolic-tangent profile (Yue *et al.* 2004):

$$\phi(x) = \phi_0(x) = \tanh\left(\frac{x}{\sqrt{2}\epsilon}\right), \tag{A 1}$$

where x is the coordinate in the direction perpendicular to the interface and $x = 0$ at the centre of the interface.

Now we impose a slow flow ($Ca = \mu V/\sigma \ll 1$) that distorts the interface, as in the devices in figure 2. Let us write

$$\phi = \phi_0 + \phi_1, \tag{A 2}$$

where ϕ_1 accounts for the deviation of ϕ from ϕ_0; ϕ_0 has the length scale ϵ, but it amounts to $G = 0$ and does not contribute to the length scale of G. So the length scale of G depends mostly on ϕ_1. Under slow-flow conditions, ϕ_1 is related to the interface curvature κ (see equation (11) of Yue *et al.* 2007):

$$\phi_1 \sim \kappa\epsilon. \tag{A 3}$$

The balance between capillary force $\sigma\kappa$ and viscous force $\mu V/l$, where l is the length scale for the variation of the flow, determines the magnitude of κ. Away from the contact line, l is the macroscopic length W, and thus $\kappa \sim Ca/W$. In the contact-line region of size $\sim l_D$, the interface curvature because of viscous bending is $\kappa \sim Ca/l_D$. As κ varies over the length scale l_D, so do ϕ_1 and G.

The upshot is that G has a length scale different from ϕ because of the higher-order nonlinear effects. For a general non-planar interface without contact line, $G \sim \sigma\kappa$

depends on the local curvature of the interface. As κ varies on a macroscopic length scale, G varies over the same macroscopic length scale rather than ϵ.

REFERENCES

Blake, T. D. 2006 The physics of moving wetting lines. *J. Colloid Interface Sci.* **299**, 1–13.

Briant, A. J. & Yeomans, J. M. 2004 Lattice Boltzmann simulations of contact line motion. Part II. Binary fluids. *Phys. Rev.* E **69**, 031603.

Caginalp, G. & Chen, X. 1998 Convergence of the phase field model to its sharp interface limits. *Eur. J. Appl. Math.* **9**, 417–445.

Cahn, J. W. 1977 Critical-point wetting. *J. Chem. Phys.* **66**, 3667–3672.

Cahn, J. W. & Hilliard, J. E. 1958 Free energy of a non-uniform system. Part I. interfacial free energy. *J. Chem. Phys.* **28**, 258–267.

Chen, H.-Y., Jasnow, D. & Viñals, J. 2000 Interface and contact line motion in a two phase fluid under shear flow. *Phys. Rev. Lett.* **85**, 1686–1689.

Cox, R. G. 1986 The dynamics of the spreading of liquids on a solid surface. Part 1. Viscous flow. *J. Fluid Mech.* **168**, 169–194.

Ding, H. & Spelt, P. D. M. 2007 Inertial effects in droplet spreading: a comparison between diffuse-interface and level-set simulations. *J. Fluid Mech.* **576**, 287–296.

Dussan, E. B. V. 1979 On the spreading of liquids on solid surfaces: static and dynamic contact lines. *Annu. Rev. Fluid Mech.* **11**, 371–400.

Fermigier, M. & Jenffer, P. 1991 An experimental investigation of the dynamic contact angle in liquid–liquid systems. *J. Colloid Interface Sci.* **146**, 226–241.

Haley, P. J. & Miksis, M. J. 1991 The effect of the contact line on droplet spreading. *J. Fluid Mech.* **223**, 57–81.

Hoffman, R. L. 1975 A study of the advancing interface. *J. Colloid Interface Sci.* **50**, 228–241.

Huang, J. J., Shu, C. & Chew, Y. T. 2009 Mobility-dependent bifurcations in capillarity-driven two-phase fluid systems by using a lattice Boltzmann phase-field model. *Intl J. Numer. Method Fluids* **60**, 203–225.

Huh, C. & Scriven, L. E. 1971 Hydrodynamic model of steady movement of a solid/liquid/fluid contact line. *J. Colloid Interface Sci.* **35**, 85–101.

Jacqmin, D. 1999 Calculation of two-phase Navier–Stokes flows using phase-field modelling. *J. Comput. Phys.* **155**, 96–127.

Jacqmin, D. 2000 Contact-line dynamics of a diffuse fluid interface. *J. Fluid Mech.* **402**, 57–88.

Jacqmin, D. 2004 Onset of wetting failure in liquid–liquid systems. *J. Fluid Mech.* **517**, 209–228.

Khatavkar, V. V., Anderson, P. D. & Meijer, H. E. H. 2006 On scaling of diffuse-interface models. *Chem. Engng Sci.* **61**, 2364–2378.

Khatavkar, V. V., Anderson, P. D. & Meijer, H. E. H. 2007 Capillary spreading of a droplet in the partially wetting regime using a diffuse-interface model. *J. Fluid Mech.* **572**, 367–387.

Koplik, J., Banavar, J. R. & Willemsen, J. F. 1988 Molecular dynamics of Poiseuille flow and moving contact lines. *Phys. Rev. Lett.* **60**, 1282–1285.

Lowengrub, J. & Truskinovsky, L. 1998 Quasi-incompressible Cahn–Hilliard fluids and topological transitions. *Proc. R. Soc. Lond.* A **454**, 2617–2654.

Mazouchi, A., Gramlich, C. M. & Homsy, G. M. 2004 Time-dependent free surface Stokes flow with a moving contact line. Part I. Flow over plane surfaces. *Phys. Fluids* **16**, 1647–1659.

Pismen, L. M. 2002 Mesoscopic hydrodynamics of contact line motion. *Colloids Surf.* A **206**, 11–30.

Qian, T., Wang, X.-P. & Sheng, P. 2003 Molecular scale contact line hydrodynamics of immiscible flows. *Phys. Rev.* E **68**, 016306.

Qian, T., Wang, X.-P. & Sheng, P. 2006*a* Molecular hydrodynamics of the moving contact line in two-phase immiscible flows. *Comm. Comput. Phys.* **1**, 1–52.

Qian, T., Wang, X.-P. & Sheng, P. 2006*b* A variational approach to moving contact line hydrodynamics. *J. Fluid Mech.* **564**, 333–360.

Renardy, M., Renardy, Y. & Li, J. 2001 Numerical simulation of moving contact line problems using a volume-of-fluid method. *J. Comput. Phys.* **171**, 243–263.

Seppecher, P. 1996 Moving contact lines in the Cahn–Hilliard theory. *Intl J. Engng Sci.* **34**, 977–992.

Sheng, P. & Zhou, M.-Y. 1992 Immiscible-fluid displacement: contact-line dynamics and the velocity-dependent capillary pressure. *Phys. Rev.* A **45**, 5694–5708.

Spelt, P. D. M. 2005 A level-set approach for simulations of flows with multiple moving contact lines with hysteresis. *J. Comput. Phys.* **207**, 389–404.

Thompson, P. A. & Robbins, M. O. 1989 Simulations of contact-line motion: slip and the dynamic contact angle. *Phys. Rev. Lett.* **63**, 766–769.

Villanueva, W. & Amberg, G. 2006 Some generic capillary-driven flows. *Intl J. Multiphase Flow* **32**, 1072–1086.

van der Waals, J. D. 1892 The thermodynamic theory of capillarity under the hypothesis of a continuous variation of density. *Verhandel Konink. Akad. Weten. Amsterdam (Sec. 1)* **1**, 1–56. Translation by J. S. Rowlingson, 1979, *J. Stat. Phys.* **20**, 197–244.

Wang, X.-P. & Wang, Y.-G. 2007 The sharp interface limit of a phase field model for moving contact line problem. *Methods Appl. Anal.* **14**, 287–294.

Yue, P., Feng, J. J., Liu, C. & Shen, J. 2004 A diffuse-interface method for simulating two-phase flows of complex fluids. *J. Fluid Mech.* **515**, 293–317.

Yue, P., Zhou, C. & Feng, J. J. 2007 Spontaneous shrinkage of drops and mass conservation in phase-field simulations. *J. Comput. Phys.* **223**, 1–9.

Yue, P., Zhou, C., Feng, J. J., Ollivier-Gooch, C. F. & Hu, H. H. 2006 Phase-field simulations of interfacial dynamics in viscoelastic fluids using finite elements with adaptive meshing. *J. Comput. Phys.* **219**, 47–67.

Zhou, M.-Y. & Sheng, P. 1990 Dynamics of immiscible-fluid displacement in a capillary tube. *Phys. Rev. Lett.* **64**, 882–885.